Photosystem I Patterning Imaged by Scanning Electrochemical Microscopy

Madalina Ciobanu,[†] Helen A. Kincaid,[‡] G. Kane Jennings,*[,‡] and David E. Cliffel*[,†]

Department of Chemistry and Department of Chemical Engineering, Vanderbilt University, Nashville, Tennessee 37235

Received July 29, 2004. In Final Form: October 26, 2004

We report the first directed adsorption of Photosystem I (PSI) on patterned surfaces containing discrete regions of methyl- and hydroxyl-terminated self-assembled monolayers (SAMs) on gold. SAM and PSI patterns are characterized by scanning electrochemical microscopy (SECM). The insulating protein complex layer blocks the electron transfer of the SECM mediator, thereby reducing the electrochemical current significantly. Uniformly and densely packed adsorbed protein layers are observed with SECM. Pattern images correlate with our previous studies where we showed that low-energy surfaces (e.g., CH_3-terminated) inhibit PSI adsorption in the presence of Triton X-100, whereas high-energy surfaces (e.g., OH-terminated) enable adsorption. Therefore, a SAM pattern with alternating methyl and hydroxyl surface regions allows PSI adsorption only on the hydroxyl surface, and this is demonstrated in the resulting SECM images.

1. Introduction

The ability to integrate biological structures with the molecular tools of materials and chemical science is a primary aim of nanobiotechnology. As systems in nature have been optimized through natural selection, a natural photodiode such as Photosystem I (PSI) can be a good candidate for studies toward nanoelectronics and molecular electronics. The PSI complex has the ability to generate photoinduced charge separation within picoseconds, a rate that is 100 times faster than that of a silicon diode.[1] Following a biomimetic approach to nanotechnology, PSI could be utilized as an integral component of molecular circuits and energy conversion systems.

Designing molecular circuits or nanocircuits relies on the ability to direct the assembly of individual functional components into desired intricate geometries that permit activity. An important aspect of integrating biomolecules into circuits and sensors[2,3] is that, upon creating patterns, the protein should retain its desired properties (e.g., functionality)[4−6] to enable interfacing with other components. Many proteins will adsorb nonspecifically on a surface and lose biological functionality due to changes in their tertiary and secondary structure. However, photosynthetic proteins have been proven to maintain some functionality and stability after adsorption on a surface.[7] This paper presents the directed assembly of PSI on patterned self-assembled monolayers (SAMs) on gold.

In nature, PSI is found in cyanobacteria as a twelve-unit supramolecular protein complex, while in green plants and algae, it has three to four additional subunits, yielding a molecular mass of ∼300 kDa.[8] The three-dimensional structure of this protein complex was recently revealed, providing structural information with atomic detail for the cyanobacterial PSI (12 protein subunits and over 100 cofactors)[9] and for the higher plant PSI (16 protein subunits and almost 200 cofactors).[10] PSI contains a specialized chlorophyll, a dimer (P700 center), that enables diode-like behavior upon excitation by photons of light.[11,12] During photosynthesis, a unidirectional transfer of electrons occurs across the thylakoid membrane; the electron-transfer vector spans from the P700 center that accepts electrons from plastocyanin to the F_A/F_B centers that donate electrons to ferredoxin.[8] Although not a trivial process, PSI can be successfully isolated from thylakoid membranes of green plants or cyanobacteria while retaining the activity of its redox centers. PSI has been the subject of recent articles[13−15] that examine its electrochemical properties. Reduction−oxidation potentials were identified for P700,[13] iron−sulfur clusters F_A/F_B, and phylloquinone A_1.[14] The photocatalytic activity of PSI was also examined in the presence of methyl viologen and cytochrome c_6.[15]

* Authors to whom correspondence should be addressed. E-mail: d.cliffel@vanderbilt.edu (D.E.C.); kane.g.jennings@vanderbilt.edu (G.K.J.). Fax: 1 (615) 322−4936 (D.E.C.); 1 (615) 343−7951 (G.K.J.).

[†] Department of Chemistry.

[‡] Department of Chemical Engineering.

(1) Lee, J. W.; Collins, R. T.; Greenbaum, E. *J. Phys. Chem. B* **1998**, *102*, 2095−2100.

(2) Nakamura, H.; Karube, I. *Anal. Bioanal. Chem.* **2003**, *377*, 446−468.

(3) Scouten, W. H.; Luong, J. H. T.; Brown, R. S. *Trends Biotechnol.* **1995**, *13*, 178−185.

(4) Wadu-Mesthrige, K.; Amro, N. A.; Garno, J. C.; Xu, S.; Liu, G. Y. *Biophys. J.* **2001**, *80*, 1891−1899.

(5) Sortino, S.; Petralia, S.; Condorelli, G. G.; Conoci, S.; Condorelli, G. *Langmuir* **2003**, *19*, 536−539.

(6) Nicolini, C. *Trends Biotechnol.* **1997**, *15*, 395−401.

(7) Wilson, M.; Kannangara, K.; Smith, G.; Simmons, M.; Raguse, B. *Nanotechnology: Basic Science and Emerging Technologies*; CRC Press, LLC: Boca Raton, FL, 2002.

(8) Chitnis, P. R. *Annu. Rev. Plant Physiol. Plant Mol. Biol.* **2001**, *52*, 593−626.

(9) Jordan, P.; Fromme, P.; Witt, H. T.; Klukas, O.; Seanger, W.; Krauss, N. *Nature* **2001**, *411*, 909−917.

(10) Ben-Shem, A.; Frolow, F.; Nelson, N. *Nature* **2003**, *426*, 630−635.

(11) He, W. Z.; Malkin, R. *Photosystems I and II*; In *Photosynthesis*, Raghavendra, A. S., Ed.; Cambridge University Press: Cambridge, 1998; pp 29−43.

(12) Lee, I.; Lee, J. W.; Greenbaum, E. *Phys. Rev. Lett.* **1997**, *79*, 3294−3297.

(13) Kievit, O.; Brudvig, G. W. *J. Electroanal. Chem.* **2001**, *497*, 139−149.

(14) Munge, B.; Das, S. K.; Ilagan, R.; Pendon, Z.; Yang, J.; Frank, H. A.; Rusling, J. F. *J. Am. Chem. Soc.* **2003**, *125*, 12457−12463.

(15) Proux-Delrouyre, V.; Demaille, C.; Leibl, W.; Setif, P.; Bottin, H.; Bourdillon, C. *J. Am. Chem. Soc.* **2003**, *125*, 13686−13692.

10.1021/la048075u CCC: $30.25
Published on Web 12/18/2004

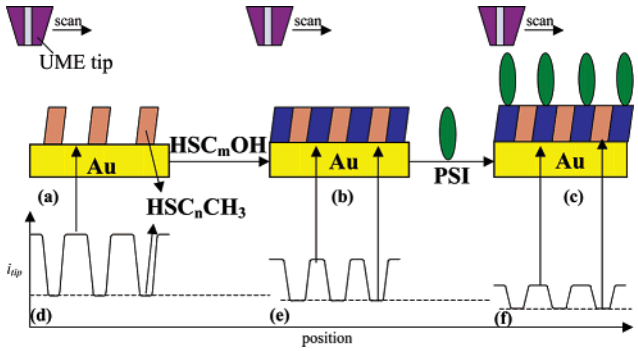

Figure 1. Schematic of PSI patterning: (a) microcontact printed SAM (e.g., CH_3-terminated ω-alkanethiol) on evaporated Au, (b) patterned SAM backfilled with OH-terminated ω-alkanethiol, and (c) patterned PSI on a chemically modified Au surface. (d–f) Current–position profiles as the UME tip scans horizontally across the patterned surface.

The ability to maintain the activity of PSI electron carriers upon isolation is inherently related to the preservation of its photodiode activity. Greenbaum and co-workers[1,12,16,17] have studied PSI both as an isolated protein and as a part of the thylakoid membrane. They investigated the orientation of PSI on chemically modified surfaces (i.e., SAMs on gold)[12] and used Kelvin force probe microscopy (KFM) to measure exogenous photovoltages generated from single PSI reaction centers on modified gold substrates.[16] They have demonstrated the photocatalytic production of hydrogen by means of platinized PSI.[1,17] Their work proves that PSI retains some activity after integration with other materials. Greenbaum and co-workers[12] also found that, on a OH-terminated surface, PSI preferentially adsorbs with its electron-transfer vector oriented upward. This particular geometry, where the P700 end of the protein is in direct contact with the SAM, appears favorable for further incorporation in molecular circuits.

Our recent work[18] demonstrates that low-energy surfaces (e.g., CH_3-terminated ω-alkanethiols) greatly inhibit the adsorption of PSI (stabilized by Triton X-100 in phosphate buffer pH 7), whereas high-energy surfaces (e.g., OH-terminated ω-alkanethiols) enable PSI adsorption. We have reasoned that the nonadsorption of PSI at low-energy surfaces is due to an adsorbed layer of Triton X-100 that orients to produce a protein-resistant poly(ethylene glycol) surface. This selectivity in adsorption suggests that PSI patterning could be achieved through a combination of microcontact printing and alkanethiol assembly in order to obtain discrete regions of 'opposing' chemical functionality where PSI will exhibit differences in adsorption. Figure 1 displays a schematic of this idea: (a) a low-energy SAM that will not allow PSI adsorption is microcontact printed on a Au surface; (b) this pattern is then backfilled with a high-energy SAM that will not only allow the PSI adsorption but will also orient the protein into a favorable configuration for further incorporation in electronics; (c) the protein adsorbs selectively on the chemically modified Au surface, yielding a PSI pattern.

Recent methods for patterning proteins include lithography and stamping techniques, ranging from thermo-

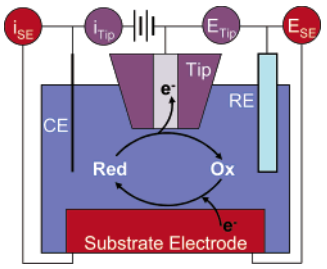

Figure 2. SECM working principle, for a conductive substrate electrode (SE): reduced species (Red) oxidized at the tip yield oxidized species (Ox); when the regeneration of Red occurs at the SE, positive feedback is observed in the form of current increase.

biolithography[19] to microcontact printing of proteins onto surfaces by direct stamping.[20–24] Perhaps the most convenient approach is to pattern a SAM that can direct the adsorption of proteins on the basis of chemical affinity.[25–27] Bhatia et al.[25] have modified organosilane SAMs by deep ultraviolet irradiation to direct IgG adsorption. Whitesides et al.[26,27] have used various techniques (e.g., micromachining, optical lithography, microcontact printing) to create patterned surfaces where proteins exhibit adsorption differences (micrometer-scale islands of alternating hydrophobic and oligo(ethylene glycol)-terminated SAMs). The protein assembled on the hydrophobic regions only since the SAMs terminated in oligo(ethylene glycol) groups resist the adsorption of proteins.[26] As shown in Figure 1, our approach also utilizes microcontact printing[28–31] to prepare a patterned surface that directs the adsorption of a protein complex (PSI) onto a surface. However, an important advantage of our approach is that commercially available methyl- and hydroxyl-terminated thiols are used to direct protein adsorption without the need for extensive synthesis of oligo(ethylene glycol)-terminated thiols. Our approach relies on the presence of the PSI-stabilizing surfactant Triton X-100, which adsorbs from solution onto low-energy (CH_3-terminated) regions to create a poly(ethylene glycol)-rich surface[18] that locally prevents PSI adsorption.

Chemical modification of surfaces and protein adsorption represent processes that modify the conductivity of substrates, making scanning electrochemical microscopy (SECM) an appropriate method for the investigation of PSI patterning. SECM is an electrochemical technique involving a four-electrode system (Figure 2), as opposed

(16) Lee, I.; Lee, J. W.; Stubna, A.; Greenbaum, E. *J. Phys. Chem. B* **2000**, *104*, 2439–2443.
(17) Millsaps, J. F.; Bruce, B. D.; Lee, J. W.; Greenbaum, E. *Photochem. Photobiol.* **2001**, *73*, 630–635.
(18) Ko, B. S.; Babcock, B.; Jennings, G. K.; Tilden, S. G.; Peterson, R. R.; Cliffel, D. E.; Greenbaum, E. *Langmuir* **2004**, *20*, 4033–4038.
(19) Fernandes, R.; Yi, H.; Wu, L.-Q.; Rubloff, G. W.; Ghodssi, R.; Bentley, W. E.; Payne, G. F. *Langmuir* **2004**, *20*, 906–913.
(20) Specht, C. G.; Williams, O. A.; Jackman, R. B.; Schoepfer, R. *Biomaterials* **2004**, *25*, 4073–4078.
(21) Bernard, A.; Delamarche, E.; Schmid, H.; Michel, B.; Bosshard, H. R.; Biebuyck, H. *Langmuir* **1998**, *14*, 2225–2229.
(22) Bernard, A.; Renault, J. P.; Michel, B.; Bosshard, H. R.; Delamarche, E. *Adv. Mater.* **2000**, *12*, 1067–1070.
(23) Tan, J. L.; Tien, J.; Chen, C. S. *Langmuir* **2002**, *18*, 519–523.
(24) Nishizawa, M.; Takoh, K.; Matsue, T. *Langmuir* **2002**, *18*, 3645–3649.
(25) Bhatia, S. K.; Teixeira, J. L.; Anderson, M.; Shriver-Lake, L. C.; Calvert, J. M.; Georger, J. H.; Hickman, J. J.; Dulcey, C. S.; Schoen, P. E.; Ligler, F. S. *Anal. Biochem.* **1993**, *32*, 197–205.
(26) Lopez, G. P.; Biebuyck, H. A.; Harter, R.; Kumar, A.; Whitesides, G. M. *J. Am. Chem. Soc.* **1993**, *115*, 10774–10781.
(27) Mrksich, M.; Chen, C. S.; Xia, Y.; Dike, L. E.; Ingber, D. E.; Whitesides, G. M. *PNAS* **1996**, *93*, 10775–10778.
(28) Tien, J.; Xia, Y.; Whitesides, G. M., Eds. *Microcontact Printing of SAMs*; Academic Press: Boston, 1998.
(29) Kumar, A.; Biebuyck, H. A.; Whitesides, G. M. *Langmuir* **1994**, *10*, 1498–1511.
(30) Odom, T. W.; Love, J. C.; Wolfe, D. B.; Paul, K. E.; Whitesides, G. M. *Langmuir* **2002**, *18*, 5314–5320.
(31) Xia, Y.; Rogers, J. A.; Paul, K. E.; Whitesides, G. M. *Chem. Rev.* **1999**, *99*, 1823–1848.

to the more common three-electrode electrochemical cells. It involves a reference electrode (RE), a counter electrode (CE), and two working electrodes (WEs): (i) a conductive substrate electrode (SE) and (ii) a tip (probe) electrode, which is in all cases an ultramicroelectrode (UME, diameter < 25 μm). SECM is an in situ scanning probe microscopy that rasters a UME tip across the surface, measuring electrochemical gradients.[32] Reversible electrochemical mediators, like ferrocenes, diffuse away from the substrate electrode and are collected electrochemically at the tip. Rastering the tip across the surface enables the mapping of conductivity and permeability of an electrode surface. Recording approach curves (ACs) to different points on a surface can also give information about conductivity differences. Usually the ACs are plotted as the normalized current (I_T = approach current i_{tip}/steady-state current i_{ss}) vs. the distance, d, between the UME and the substrate. The expression for i_{ss} is given by

$$i_{ss} = 4nFDCa \quad (1)$$

where n is the number of electrons, F is the Faraday constant, D and C are the diffusion coefficient and the concentration for the electrochemically active species, respectively, and a is the radius of the UME.[32] The UME can travel vertically, as in the case of recording ACs, or horizontally, as in the case of imaging. For the case of a conductive substrate and a perfectly reversible redox couple, the potentials (E_{tip} and E_{SE}) would be set such that the mediator would undergo oxidation at one of the electrodes and reduction at the other one (e.g., oxidation at the UME and reduction at the SE). When the UME is far from the substrate (>tens of micrometers), i_{ss} reaches a constant value that is limited by the diffusion of the redox species to the disk-shaped UME. When the distance between the two electrodes is within a few micrometers, a positive feed-back loop is created, wherein the oxidized mediator (Ox) produced at the tip will quickly diffuse to the SE, where it will undergo the reduction reaction, and the reduced species (Red) will diffuse back to the UME (Figure 2). As the distance between electrodes decreases, this electrochemical cycling will increase, and the tip current will exhibit a sharp increase and hence provide a positive feedback signal, with a few hundred percent increase for a final approach of the UME to within a few micrometers of the SE. For the case of an insulating substrate, as the two electrodes approach within micrometers, the tip current will decrease as the proximity of the two electrodes blocks diffusion to the tip, providing a negative feedback signal. A positive feedback approach current is considered maximum (I_{Tmax}) right before the tip contacts the substrate. A more-conductive surface will result in a larger maximum approach current, and this maximum can typically approach 800% of i_{ss} on purely conductive surfaces (I_T = 8). ACs to a completely insulating surface will present only I_T values <1, with the current decreasing continuously as the tip approaches the substrate surface. When the tip travels horizontally, as in the case of SECM imaging, the output of the instrument is a current−position profile for the surface scanned. Figure 1d−f depicts a schematic of how such profiles would appear for patterned surfaces. An SECM image is a collection of current−position profiles.

SECM has been previously used for the study of microcontact printed surfaces, providing important information regarding density and uniformity of adsorption, as well as images of patterns where differences in conductivity are highlighted. Wilhelm and Wittstock[33] have used the SECM for the study of enzyme patterns on microcontact printed SAMs. They obtained images with good resolution when using longer-chained thiols (C_{16}−C_{20}), but for chain lengths under C_{12}, the resolution was very poor and the patterns could not be distinguished. They have also used SECM for local electrochemical desorption of SAMs to pattern and study functional proteins.[34] Additionally, Matsue et al.[24] have used PDMS stamps to pattern fibronectin on glass substrates in order to promote cell growth, and they employed SECM to study the respiration of patterned HeLa cells.

This paper will address patterning methods for PSI to enable future prototype microscale devices containing nanoscale components. By utilizing the unique adsorption characteristics of PSI on chemically modified substrates, we generate patterns through bottom-up assembly using the simplistic and inexpensive technique of microcontact printing. Since alternating regions on the patterned surfaces present different conductivities, we utilize SECM approach curves and imaging to assess the formation of PSI patterns on a substrate.

2. Experimental Section

2.1. Materials. The chemicals were purchased as follows: $Na_4P_2O_7 \cdot H_2O$, $MgCl_2 \cdot 6H_2O$, $NaH_2PO_4 \cdot H_2O$, HCl, $MnCl_2 \cdot 4H_2O$, NaCl, KCl, $K_3Fe(CN)_6$, 30% H_2O_2, and acetone from Fisher Scientific; 11-mercapto-1-undecanol ($HSC_{11}OH$), KPF_6, and EDTA from Aldrich Chemical; 1-dodecanethiol ($HSC_{11}CH_3$), sorbitol, ascorbic acid, Triton X-100, HEPES, hexaammineruthenium(III) cloride, and Tricine from Acros; $Na_2HPO_4 \cdot 7H_2O$, sodium ascorbate, and DL-dithiothreitol from Sigma; H_2SO_4 and NaOH from EM Science; ethanol (absolute proof) from Aaper; hydroxylapatite fast-flow from Calbiochem; 6-mercapto-1-hexanol (HSC_6OH) from Fluka; ferrocenylmethyltrimethylammonium iodide from Strem Chemicals; N_2 from Gibbs Welding Supply; conductive silver epoxy from Epoxy Technology; and white sealant Hysol Epoxi-Patch from Dexter Corporation. All chemicals were used as received unless otherwise specified.

ASTM Type I (18 MΩ) analytical grade deionized water (DW) was obtained with a Solution 2000 Water Purification System from Solution Consultants. All solutions were filtered prior to use with 0.2 μm syringe filters from Fisher. Ferrocenylmethyltrimethylammonium hexafluorophosphate (FcTMA) was prepared according to the method of Mirkin and co-workers.[35]

Gold shot (99.99%) and chromium-coated tungsten filaments were obtained from J&J Materials and R. D. Mathis, respectively. Silicon (100) wafers (p-doped with boron) were obtained from Montco Silicon. Sylgard 184 silicone elastomer base and curing agent were purchased from Dow Corning Corporation. Gold interdigitated arrays (Au IDAs) with 10 μm Au lines separated by 10 μm glass lines were obtained from Abtech Scientific, Inc.

2.2. Preparation of Evaporated Gold Substrates. Silicon (100) wafers were rinsed with ethanol, DW, and dried with N_2. Au substrates were prepared by evaporating chromium (100 Å) and Au (1250 Å) in sequence onto the wafers at rates of 1−2 Å/s in a diffusion-pumped chamber with a base pressure of 4×10^{-6} Torr. After removal from the evaporation chamber, the Au-coated wafers were cut into 2 cm × 2 cm pieces and connected to a copper contact wire with the aid of conducting silver epoxy. The connection was further isolated with epoxy sealant. The Au surface was cleaned with piranha solution (3:1 concentrated H_2SO_4/30% H_2O_2) prior to use (*CAUTION!!! Piranha solution is to be handled only in the hood using appropriate protective equipment.*), thoroughly rinsed with DW then ethanol, and dried in N_2. A fresh piece of Au was used in each experiment to eliminate errors that could be introduced by possible surface damage.

(32) Bard, A. J., Fan, F. R. F., Mirkin, M. V., Eds. *Scanning Electrochemical Microscopy*; Marcel Dekker: New York, 1994.

(33) Wilhelm, T.; Wittstock, G. *Langmuir* **2002**, *18*, 9485−9493.

(34) Wilhelm, T.; Wittstock, G. *Electrochim. Acta* **2001**, *47*, 275−281.

(35) Forouzan, F.; Bard, A. J.; Mirkin, M. V. *Isr. J. Chem.* **1997**, *37*, 155−163.

2.3. Photosystem I Extraction and Characterization. Commercial spinach leaves were used for the isolation of thylakoid membranes according to Reeves and Hall.[36] Further separation and isolation of native PSI involved a hydroxylapatite column previously described by Shiozawa et al.[37] and Lee et al.[16,38] The PSI suspension in 200 mM phosphate buffer pH 7, containing 1 mM Triton X-100 was stored at −80 °C.[39] The extract contained PSI 40 (40 chlorophyll molecules per P700 center), and it was characterized for chlorophyll concentration using 80% acetone,[40] while the P700 concentration was determined by monitoring the chemically induced absorbance change (recording oxidized minus reduced spectra) as described by Baba et al.[41] The absorbance change procedure was modified by using 50 mM ferrocyanide[39] and dithiothreitol as the electron donor[42] instead of 2,6-dichlorophenol indophenol.

2.4. Scanning Electrochemical Microscopy. SECM measurements were conducted with a CHI900 instrument from CH Instruments equipped with an adjustable stage for tilt correction. The electrochemical cell was in a typical four-electrode configuration: UME tip electrode, Pt wire counter electrode, Ag/AgCl, 3 M KCl reference electrode (CHI111), and substrate electrode, which was either a 2 mm Pt disk (CHI303) for UME testing or evaporated Au for imaging. All UMEs were manufactured with 5 μm Pt wire from Goodfellow according to Bard et al.,[32] polished with 0.05 μm alumina from Buehler, and sonicated in ethanol and water. The actual measured radius for the UMEs was a = 3.5 μm (see eq 1). UMEs were electrochemically cleaned for 5 min in 0.5 M H_2SO_4 using a CHI660a potentiostat and were tested with 1 mM FcTMA in 100 mM KCl for performance. The Pt SE was polished and cleaned in an identical manner to the UMEs. The SECM images were considered valid if the UME approached before and after imaging a Pt SE at $I_T = 8$. This was done to ensure that no significant electrode fouling took place during the experiments. The UMEs were also characterized by cyclic voltammetry (CV) and consistently yielded the expected sigmoidal CV. For imaging on evaporated Au substrates, the mediator was 1 mM FcTMA in 200 mM pH 7 phosphate buffer with 1 mM Triton X-100. For imaging on Au IDAs, the mediator was 1 mM FcTMA in 100 mM KCl. All PSI imaging was conducted in the dark at room temperature.

I_{Tmax} values were recorded in Table 1 for patterns to demonstrate backfilling. The I_{Tmax} values refer to the specific images presented in this paper. On each studied surface, we investigated at least three distinct points for each pattern component (e.g., for Figure 5a, we have taken into account three approach curves to the Au regions and three approach curves to the C_{12} regions); more commonly, four or five different values were averaged, and the data are presented with the corresponding standard deviation.

All SECM images were acquired in the constant height mode. The ACs served as means of positioning the tip close to the surface before acquiring an SECM image. For example, when approaching a 7.0 μm tip to a perfectly conductive surface in the presence of a reversible electrochemical mediator, for an approach current $I_T = 2.0$, the tip is at $d = 2.2$ μm from the SE. Distances within a few micrometers will yield good resolution images. For the cases when the I_{Tmax} values were determined, it was possible to estimate the tip to SE distance, d. Since each pattern has two types of surfaces, it was important to know to which region the approach was done before recoding each image. For example, in the case when we approached to Au before imaging at a current value $I_T = 2$, knowing that $I_{Tmax} = 4.2$, we used the approach curve for which I_{Tmax} was found to measure the distance between the 0 μm point and the point corresponding to $I_T = 2$ and found $d = 1.38$ μm.

For all SECM images presented in this paper, we have the following common experimental parameters: $a = 3.5$ μm; RG = 5 ± 0.5; $E_{tip} = +0.65$ V, $E_{SE} = 0$ V, vs. Ag/AgCl, 3 M KCl; imaging scan rate: 30 μm/s; the concentration of FcTMA was approximately 1 mM; for each image, the i_{ss} value is provided in the figure caption and the exact concentration of the mediator can be easily calculated using eq 1 since all other parameters are known.

2.5. Microcontact Printing. Stamps were fabricated in a clean room using lithographic masters (photoresist pattern on silicon) donated by Professor Ki-Bum Kim (Seoul National University). By volume, one part of elastomer curing agent to 10 parts of elastomer base were mixed thoroughly and then placed under vacuum in order to purge any entrapped air. The mixture was then poured onto the masters and cured in a 60 °C oven for 2 h. The PDMS stamps were cut into their respective sizes (~10 mm × 10 mm) using a scalpel.

PDMS stamps were thoroughly rinsed with ethanol and dried in N_2 prior to using a cotton swab (Hardwood Products Company LLC) to apply a 4 mM ethanolic solution of the thiol across the patterned surface of the stamp. The stamp was dried with N_2 and then placed onto the flat Au surface for 30 s. If backfilling was required, the patterned Au surface was dried 30 min in open air and then immersed in a 1 mM ethanolic solution of a different ω-terminated alkanethiol for 10 min. The patterned Au was rinsed and then sonicated for 5 s in ethanol and dried in N_2.

To confirm successful pattern transfer from PDMS to the Au surface, stamped surfaces (not backfilled) were exposed to an etching solution of 1 mM $K_3Fe(CN)_6$ and 100 mM KCN[29] in DW (60 mL soln/cm^2 of Au) and stirred.[43] Substrates were then thoroughly rinsed with DW, dried in N_2, and observed with an Olympus BX41 optical microscope to verify that etching was limited to the exposed Au regions.

For PSI adsorption, the patterned Au substrate, or the Au IDA (already modified by overnight exposure to 1 mM $HSC_{11}OH$ in ethanol) was placed overnight (~20 h) in the dark at 4 °C in a PSI solution containing ~50 μg chlorophyll/mL and 1 mM Triton X-100. Before use, the substrates were briefly rinsed with DW and dried in a gentle stream of N_2.

2.6. Reflectance−Absorption Infrared Spectroscopy (RAIRS). RAIRS was performed using a Bio-Rad Excalibur FTS-3000 infrared spectrometer. The p-polarized light was incident at 80° from the surface normal. The instrument was run in single-reflection mode and equipped with a universal sampling accessory. A liquid-nitrogen-cooled, narrow-band mercury cadmium telluride detector was used to detect reflected light. Spectral resolution was 2 cm^{-1} after triangular apodization. Each spectrum was accumulated over 1000 scans with a deuterated octadecanethiol d_{37} SAM on flat gold as the background. The presence of water was minimized by flowing nitrogen gas through the sample compartment at a flow rate of roughly 6 standard liters per minute for at least 30 min. A water spectrum was created by rescanning the perdeuterated background sample in the presence of water vapor, and it was subtracted from the spectrum of each sample to better resolve the peaks of interest in the 1200−1900 cm^{-1} region.

3. Results and Discussion

PSI adsorption on chemically modified Au surfaces was investigated with SECM. The first substrate studied was a Au IDA in which Au lines are interdigitated on an insulating glass substrate. Au IDAs allow for a good control between completely conductive and insulating regions to provide model substrates for SECM studies. Sets of ACs were recorded with each modification of the IDA. Figure 3a displays the SECM image and AC of a Au IDA after electrochemical cleaning, using a Pt tip and FcTMA as mediator. The image was recorded after approaching at $I_T = 2$ to the Au; the shape of the AC was consistent with a conductive Au surface. After assembly of the $HOC_{11}S$− monolayer on Au, highly conductive feedback is no longer

(36) Reeves, S. G.; Hall, D. O. *Methods Enzymol.* **1980**, *69*, 85−94.
(37) Shiozawa, J. A.; Alberte, R. S.; Thornber, J. P. *Arch. Biochem. Biophys.* **1974**, *165*, 388−397.
(38) Lee, J. W. Ph.D. Dissertation, Cornell University, 1993.
(39) Hui, Y.; Jie, W.; Carpentier, R. *Photochem. Photobiol.* **2000**, *72*, 508−512.
(40) Arnon, D. I. *Plant Physiol.* **1949**, *24*, 1−15.
(41) Baba, K.; Itoh, S.; Hastings, G.; Hoshina, S. *Photosynth. Res.* **1996**, *47*, 121−130.
(42) Krasnovsky, A. A.; Ni, C. V.; Nikandrov, V. V.; Brin, G. P. *Plant Physiol.* **1980**, *66*, 925−930.
(43) Zhao, X.-M.; Wilbur, J. L.; Whitesides, G. M. *Langmuir* **1996**, *12*, 3257−3264.

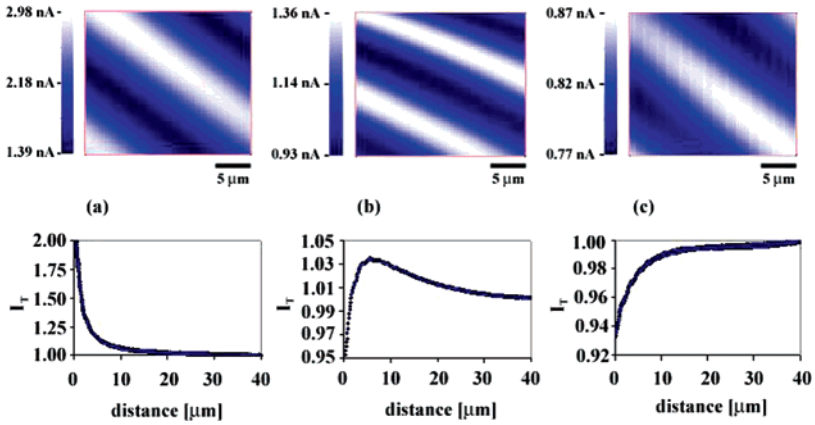

Figure 3. SECM images of Au IDAs using FcTMA and a 7 μm Pt tip: (a) Au IDA image with corresponding AC to the Au digit; $i_{ss} = 0.94$ nA; tip positioned by AC to Au, $I_T = 2$; (b) IDA with SAM on Au digits, and corresponding AC to the Au−$SC_{11}OH$ region; $i_{ss} = 1.07$ nA; tip positioned by AC to $C_{11}OH$, $I_T = 0.94$; (c) image of adsorbed PSI on a high-energy surface, $HSC_{11}OH$, and the corresponding AC to the PSI region; $i_{ss} = 0.93$ nA; tip positioned by AC to PSI, $I_T = 0.94$. On all images the lowest current corresponds to the glass part from the IDAs.

observed at any point on the IDA, as the AC indicates only partial conductivity (Figure 3b). Generally, any I_T value above unity indicates some positive feedback from a conductive substrate. The corresponding image from Figure 3b presents a lower overall current with a smaller difference between the SAM (higher current values) and the glass (lower current values): 435 pA (3b) vs. 1.59 nA (3a). In comparison to Figure 3b, overnight PSI adsorption (Figure 3c) demonstrates a more dramatic loss in current and contrast (only 96 pA) relative to the previous image (Figure 3b), owing to the presence of the protein layer. At this point, all ACs have the characteristic trend of an insulating surface (Figure 3c) due to the adsorbed PSI. Although the entire surface appears to be insulating, the glass still exhibits the lowest current since the incomplete coverage of PSI allows some mediator faradaic current through the exposed SAM. It was not possible to fit the recorded ACs to the existing theoretical ACs since in our case the substrate is patterned, causing mixed positive and negative feedback interference from the adjacent pattern lines. The approach curve fitting theories have been developed only for uniform substrates (i.e., nonpatterned). We note that the images presented in Figure 3 are for the same Au IDA. Although we have not defined the zero point for the ACs in Figure 3, we were able to compare the images with respect to their current and contrast. The SECM mode that we use for imaging is the constant height mode. The 'constant height' is set approaching the substrate to a certain feedback current level. For Figure 3b and c, for example, we have used the same approach current level ($I_T = 0.94$) for positioning the tip before acquiring the images. To be able to compare the feedback levels, we have approached the same type of region on the IDA, i.e., the high-current region corresponding to the modified Au digits. Thus, if there is no difference in the patterns, the images should look identical; this is not the case in Figure 3b and c. We observe that, for the same feedback level in positioning the tip near the substrate, Figure 3c corresponds to a substrate that is more insulating overall.

We obtained similar results to the ones presented in Figure 3 for a different redox mediator, hexaammineruthenium(III) chloride ($E_{tip} = -0.35$ V, $E_{SE} = 0$ V, vs. Ag/AgCl, 3 M KCl), while degassing the solution. Since the SECM studies appeared independent of the type of redox mediator, we chose FcTMA for all the other experiments.

We have also used SECM to image the directed adsorption of PSI at surfaces containing discrete regions of CH_3- and HO-terminated SAMs on Au created by microcontact printing and subsequent backfilling. The patterned SAMs on Au were investigated by SECM immediately after each step of stamping, backfilling with a different SAM, and PSI adsorption. No ACs are shown for this study since they all have the indicative trend for a conductive substrate (Supporting Information, Figure 3); I_{Tmax} values are given instead. SECM imaging of stamped short-chained ω-alkanethiolate SAMs (e.g., HSC_6OH) does not yield distinguishable differences between the Au and the SAM due to the insufficient insulating capacity of the thin SAM. Complimentary experiments indicate no preferential rate of etching between Au and this type of SAM. This is a consequence of inefficient packing of short-chained ω-alkanethiols that results from their decreased van der Waals interactions between adjacent hydrocarbon chains (disorganized SAMs appear to be less insulating). Longer-chained SAMs prepared from $HSC_{11}OH$ or $HSC_{11}CH_3$ result in SECM images indicative of successful patterning (in accordance with results from etching experiments). The CH_3-terminated SAMs are more insulating than the OH-terminated SAMs because the alkyl-terminated thiols form more-organized SAM blocking layers. Figure 4a displays the SECM image of a 10 μm line pattern of $HSC_{11}OH$ with 20 μm spacings of Au, where a lower current is observed for the insulating SAM. Upon backfilling this particular pattern with $HSC_{11}CH_3$, the 20 μm lines now become more insulating than the 10 μm lines ($HSC_{11}OH$), indicating that the hydrophobic monolayer impedes the flow of electrochemical mediator current at the substrate to a greater extent than a hydrophilic monolayer of the same overall chain length (Figure 4b). Exposing this backfilled pattern to a PSI solution results in the selective adsorption of the protein onto the hydroxyl regions, which causes reduced currents and loss of image contrast in Figure 4c. The thickness of the insulating protein layer blocks the electron transfer, thereby reducing the electrochemical current significantly.

When comparing two images taken in similar conditions, it is important to know the relative position of the tip with respect to the substrate. For the case presented in Figure 4, regardless of the tip to substrate distance, d, we can easily assess that the backfilling occurred since the Au−$SC_{11}OH$ regions went from low-current (Figure 4a) to high-current (Figure 4b). The tip positioning in the proximity of the substrate was done by ACs: for Figure 4a we approached on the Au−$SC_{11}OH$ region to a current value

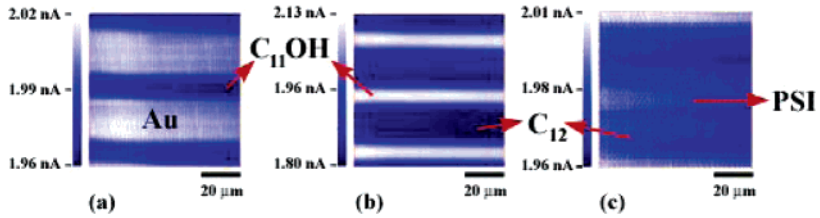

Figure 4. SECM images of microcontact patterned gold using FcTMA as mediator with a 7 μm Pt tip: (a) 10 μm $HSC_{11}OH$ with 20 μm Au lines; $i_{ss} = 1.02$ nA; tip positioned by AC to $C_{11}OH$, $I_T = 2$; (b) 10 μm $HSC_{11}OH$ backfilled with 20 μm $HSC_{11}CH_3$ lines $i_{ss} = 0.98$ nA; tip positioned by AC to C_{12}, $I_T = 1.75$; (c) 10 μm PSI lines (adsorbed onto $HSC_{11}OH$) spaced by 20 μm $HSC_{11}CH_3$ lines; $i_{ss} = 0.99$ nA; tip positioned by AC to PSI, $I_T = 2$.

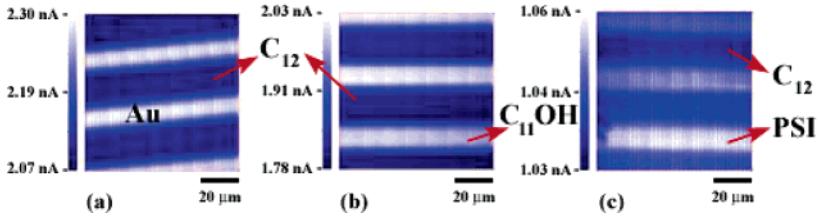

Figure 5. SECM images of microcontact patterned gold using FcTMA as mediator with a 7 μm Pt tip: (a) 20 μm $HSC_{11}CH_3$ was patterned initially, with 10 μm Au line gaps; $i_{ss} = 1.07$ nA; $d = 1.38$ μm; tip positioned by AC to Au, $I_T = 2$; (b) 20 μm $HSC_{11}CH_3$ backfilled with 10 μm $HSC_{11}OH$ lines; $i_{ss} = 1.11$ nA; $d = 0.92$ μm; tip positioned by AC to $C_{11}OH$, $I_T = 2$. The current is lower in both cases for the CH_3-terminated SAM, but the maximum approach current (lower in (b)) indicates that backfilling was successful; (c) 10 μm PSI lines (adsorbed onto $HSC_{11}OH$) spaced by 20 μm $HSC_{11}CH_3$ lines; $i_{ss} = 0.85$ nA; $d = 0.41$ μm; tip positioned by AC to Au, $I_T = 1.4$. The overall lower current indicates successful PSI adsorption.

$I_T = 2$, while for Figure 4b we approached on the Au−$SC_{11}CH_3$ region to a current value $I_T = 1.75$. For the same value for I_T, if we compare a perfectly conductive substrate with a SAM-modified substrate, the tip will be closer to the substrate in the case of the modified SE. A comparison between the images in parts b and c of Figure 4 is relevant only if the tip was at least as close to the SE in 4c as it was in 4b. Since in 4b the approach current before imaging was at $I_T = 1.75$, the tip was at least as close to the SE in 4c since it was positioned through an $I_T = 2$ (we estimate that the tip was actually closer to the SE in 4c than in 4b).

Since the monolayers assembled from solutions have different electrochemical properties than the SAMs obtained through microcontact printing,[44] we investigated the effect of the stamping/backfilling order on the properties of the pattern and on the protein adsorption. Initial patterning with $HSC_{11}CH_3$ yields 20 μm lines of insulating SAM and 10 μm lines of Au (Figure 5a), while the backfilling of this surface with $HSC_{11}OH$ is displayed in Figure 5b. In both a and b of Figure 5, the lower current corresponds to the low-energy surface. Approaching points at various locations on the patterned surface demonstrates successful backfilling. On the initial pattern (Figure 5a), the tip was able to approach at a maximum current $I_{Tmax} = 4.2$ on the 10 μm Au lines. Table 1 presents I_{Tmax} values for the patterns presented in Figures 5 and 6, and it specifies for which pattern region the AC was recorded. Although Au is a conductive surface, the current cannot reach higher values due to diffusional hindrance of the electrochemical mediator caused by the tip size (the 7 μm Pt wire is insulated in glass, and the entire diameter of the tip is ~ 35 μm) and the adjacent SAM lines; the shape of the normal diffusional plume at the UME is altered by the presence of the SAM lines that border the Au region on two sides. On the backfilled pattern (Figure 5b), the low-energy surface decreases the I_{Tmax} value from 3.2 to 2.2 due to the fact that the 10 μm gaps are now filled with a SAM that is inherently less conductive than Au. The ACs to these 10 μm $HOC_{11}S$− lines give a much lower

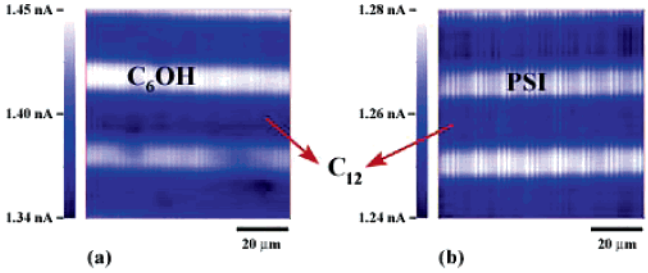

Figure 6. SECM images of SAM-modified Au and patterned PSI using FcTMA and a 7 μm Pt tip: (a) 20 μm $HSC_{11}CH_3$ backfilled with 10 μm HSC_6OH lines; $i_{ss} = 0.89$ nA; $d = 1.05$ μm; tip positioned by AC to C_{12}, $I_T = 1.5$; (b) 10 μm PSI lines (adsorbed onto HSC_6OH) spaced by 20 μm $HSC_{11}CH_3$ lines; $i_{ss} = 0.82$ nA; $d = 0.51$ μm; tip positioned by AC to C_{12}, $I_T = 1.5$. The maximum approach current I_{Tmax} is similar in both cases, but the lower current in (b) indicates the presence of PSI.

overall current ($I_{Tmax} = 3.1$) than that reported in Figure 5a. The values of the approach currents for each type of surface in each individual pattern prove that the backfilling of an ω-alkanethiol with a different terminal group was successfully achieved.

The backfilled pattern of Figure 5b was used to study the PSI adsorption, and the resulting image is presented in Figure 5c. ACs are recorded in different locations, and the maximum value reached anywhere on the surface was $I_{Tmax} = 1.5$, demonstrating that the surface becomes more insulating in its entirety upon PSI adsorption. Since PSI does not cover the OH-terminated surface completely,[12] some electrochemical mediator current is still observed, rendering the OH-terminated surface slightly more electrochemically active than the CH_3-terminated surface. Once the PSI is adsorbed, the image contrast decreases from 250 pA for the backfilled pattern to 30 pA for the patterned PSI. The image in Figure 5c, although it still displays the lowest current for $HSC_{11}CH_3$, does have PSI adsorbed on the surface. It is important to notice that with each image presented in Figure 5 we had to bring the tip closer to the substrate to be able to distinguish the pattern: d is 1.38 μm for 5a, 1.11 μm for 5b, and 0.41 μm for 5c. After imaging, each piece of patterned Au was

(44) Losic, D.; Shapter, J. G.; Gooding, J. J. *Langmuir* **2001**, *17*, 3307−3316.

Table 1. I_T Maximum Values for Different Patterned Surfaces

Au surface stamped with C_{12}	I_{Tmax} for approach curves to					
and backfilled with $C_{11}OH$ (Figure 5)	(a) −Au	(a) $-C_{12}$	(b) $-C_{11}OH$	(b) $-C_{12}$	(c) −PSI	(c) $-C_{12}$
	4.2 ± 0.1	3.2 ± 0.4	3.1 ± 0.2	2.2 ± 0.4	1.45 ± 0.03	1.47 ± 0.04
and backfilled with C_6OH (Figure 6)	(a) $-C_6OH$	(a) $-C_{12}$	(b) −PSI	(b) $-C_{12}$	N/A	
	2.0 ± 0.1	1.6 ± 0.1	2.4 ± 0.1	2.0 ± 0.2		

subjected to RAIRS analysis, and in every case, the characteristic amide bands[18] (not shown) were detected, indicating definite PSI adsorption on the patterned surface. Our previous work has shown that PSI adsorbs only on high-energy surfaces (e.g., hydroxyl-terminated) but not on low-energy surfaces (e.g., methyl-terminated) in the presence of Triton X-100.[18]

PSI adsorption on a $HOC_{11}S-$ pattern backfilled with $HSC_{11}CH_3$ (Figure 4c) contrasts that on a $CH_3C_{11}S-$ pattern backfilled with $HSC_{11}OH$ (Figure 4c). As the patterning and the backfilling order influences the conductivity of the pattern, the adsorption of PSI is expected to be influenced as well. Losic et al.[44] have shown that a stamped SAM and a solution-formed SAM differ in their electrochemical behavior; a stamped monolayer is less organized, resulting in a more-conductive surface. The hydroxyl-terminated SAM is more insulating when it is assembled (Figure 5) than when it is stamped (Figure 4). This difference is consistent with more PSI adsorption onto the stamped, inferior SAM (Figure 4c). Figure 5c displays improved resolution (as compared with Figure 4c), suggesting a reduced coverage of PSI that allows more current.

Since the ultimate goal of this research is the implementation of PSI in nanocircuits, we also investigated whether PSI adsorption can be directed on short-chained SAMs, where the protein would be closer to the conductive Au, providing less resistance to electron transfer. Figure 6a shows an SECM image of a surface after stamping with $HSC_{11}CH_3$ and backfilling with HSC_6OH, which is similar to that observed when backfilling with $HSC_{11}OH$. Although the ACs recorded for the backfilled pattern (Figure 6a) and for the patterned protein (Figure 6b) do not exhibit notable differences, the reduced contrast (110 pA (6a) to 40 pA (6b)) indicates that the PSI adsorption lowers the overall current. Since PSI adsorption reduces mediator currents, to achieve the reduced contrast in Figure 6b, we had to bring the tip half a micrometer closer to the SE than for the image displayed in Figure 6a.

When SECM is used to characterize the directed adsorption of PSI at patterned surfaces, the electrochemical surface image provides information about the uniformity of adsorption. Since the PSI regions in most of the presented images appear uniform and the current is significantly reduced, we infer that the protein layers are uniformly adsorbed (across the scale of micrometers) and densely packed (on the scale of nanometers) on the hydroxyl surfaces. In Figure 6a, the bottom $Au-SC_6OH$ line is not uniform, indicating that the SAM is probably not packed to the same extent across the imaged region. However, Figure 6b displays uniform current bands for PSI, which along with the dramatic loss in conductivity, suggest a densely packed protein layer. These densely packed layers are confirmed in all images by large changes in current and contrast.

4. Conclusions

We report the first directed assembly of PSI on model surfaces prepared through microcontact printing and its characterization by SECM. Patterning of SAMs enables the creation of discrete regions of chemical functionality on Au surfaces for selective adsorption of PSI. SECM is employed for electrochemical imaging of patterned surfaces because it can detect changes in the conductivity of a surface upon the formation of SAMs on evaporated Au, as well as the changes in the conductivity upon backfilling of the initial pattern and adsorption of PSI.

Acknowledgment. We gratefully acknowledge a Vanderbilt Discovery Grant and the Vanderbilt Institute of Nanoscale Science and Engineering for supporting this work. We thank B. Samuel Ko (Vanderbilt) and Professor Ki-Bum Kim (Seoul National University) for providing masters. We also acknowledge Professor John P. Wikswo for access to clean room facilities and Ron Reiserer for his aid in the fabrication of PDMS stamps.

Supporting Information Available: (i) Supplemental discussion and data supporting the statement that PSI does not adsorb on the low-energy (methyl-terminated) regions of the pattern and (ii) supplemental figure displaying examples of approach curves for the images presented in Figure 4. This material is available free of charge via the Internet at http://pubs.acs.org.

LA048075U